Class XI Myosins Move Specific Organelles in Pollen Tubes and Are Required for Normal Fertility and Pollen Tube Growth in Arabidopsis[1][OPEN]

Stephanie L. Madison, Matthew L. Buchanan, Jeremiah D. Glass, Tarah F. McClain, Eunsook Park[2], and Andreas Nebenführ*

Department of Biochemistry and Cellular and Molecular Biology, University of Tennessee, Knoxville, Tennessee 37996–0840

ORCID ID: 0000-0003-2984-3039 (E.P.).

Pollen tube growth is an essential aspect of plant reproduction because it is the mechanism through which nonmotile sperm cells are delivered to ovules, thus allowing fertilization to occur. A pollen tube is a single cell that only grows at the tip, and this tip growth has been shown to depend on actin filaments. It is generally assumed that myosin-driven movements along these actin filaments are required to sustain the high growth rates of pollen tubes. We tested this conjecture by examining seed set, pollen fitness, and pollen tube growth for knockout mutants of five of the six myosin XI genes expressed in pollen of Arabidopsis (*Arabidopsis thaliana*). Single mutants had little or no reduction in overall fertility, whereas double mutants of highly similar pollen myosins had greater defects in pollen tube growth. In particular, *myo11c1 myo11c2* pollen tubes grew more slowly than wild-type pollen tubes, which resulted in reduced fitness compared with the wild type and a drastic reduction in seed set. Golgi stack and peroxisome movements were also significantly reduced, and actin filaments were less organized in *myo11c1 myo11c2* pollen tubes. Interestingly, the movement of yellow fluorescent protein-RabA4d-labeled vesicles and their accumulation at pollen tube tips were not affected in the *myo11c1 myo11c2* double mutant, demonstrating functional specialization among myosin isoforms. We conclude that class XI myosins are required for organelle motility, actin organization, and optimal growth of pollen tubes.

Pollen tubes play a crucial role in flowering plant reproduction. A pollen tube is the vegetative cell of the male gametophyte. It undergoes rapid polarized growth in order to transport the two nonmotile sperm cells to an ovule. This rapid growth is supported by the constant delivery of secretory vesicles to the pollen tube tip, where they fuse with the plasma membrane to enlarge the cell (Bove et al., 2008; Bou Daher and Geitmann, 2011; Chebli et al., 2013). This vesicle delivery is assumed to be driven by the rapid movement of organelles and cytosol throughout the cell, a process that is commonly referred to as cytoplasmic streaming (Shimmen, 2007). Cytoplasmic streaming in angiosperm pollen tubes forms a reverse fountain: organelles moving toward the tip travel along the cell membrane, while organelles moving away from the tip travel through the center of the tube (Heslop-Harrison and Heslop-Harrison, 1990; Derksen et al., 2002). Drug treatments revealed that pollen tube cytoplasmic streaming and tip growth depend on actin filaments (Franke et al., 1972; Mascarenhas and Lafountain, 1972; Heslop-Harrison and Heslop-Harrison, 1989; Parton et al., 2001; Vidali et al., 2001). Curiously, very low concentrations of actin polymerization inhibitors can prevent growth without completely stopping cytoplasmic streaming, indicating that cytoplasmic streaming is not sufficient for pollen tube growth (Vidali et al., 2001). At the same time, however, drug treatments have not been able to specifically inhibit cytoplasmic streaming; thus, it is unknown whether cytoplasmic streaming is necessary for pollen tube growth.

Myosins are actin-based motor proteins that actively transport organelles throughout the cell and are responsible for cytoplasmic streaming in plants (Shimmen, 2007; Sparkes, 2011; Madison and Nebenführ, 2013). Myosins can be grouped into at least 30 different classes based on amino acid sequence similarity of the motor domain, of which only class VIII and class XI myosins are found in plants (Odronitz and Kollmar,

[1] This work was supported by the National Science Foundation (grant no. MCB–0822111 to A.N. and a Pollen Research Coordination Network on Integrated Pollen Biology grant to S.L.M. to attend the Basic Methods in Pollen Research Course at Brown University).

[2] Present address: Department of Plant Biology and Genome Center, 3111 Life Sciences, University of California, Davis, CA 95616.

* Address correspondence to nebenfuehr@utk.edu.

The author responsible for distribution of materials integral to the findings presented in this article in accordance with the policy described in the Instructions for Authors (www.plantphysiol.org) is: Andreas Nebenführ (nebenfuehr@utk.edu).

S.L.M. and A.N. conceived the project and designed the experiments; E.P. and S.L.M. isolated the myosin knockout mutants; S.L.M., M.L.B., J.D.G., T.F.M., and A.N. performed the experiments; S.L.M. and A.N. analyzed the data and wrote the article.

[OPEN] Articles can be viewed without a subscription.

www.plantphysiol.org/cgi/doi/10.1104/pp.15.01161

2007; Sebé-Pedrós et al., 2014). Class VIII and class XI myosins have similar domain architecture. The N-terminal motor domain binds actin and hydrolyzes ATP (Tominaga et al., 2003) and is often preceded by an SH3-like (for sarcoma homology3) domain of unknown function. The neck domain, containing IQ (Ile-Gln) motifs, acts as a lever arm and is bound by calmodulin-like proteins that mediate calcium regulation of motor activity (Kinkema and Schiefelbein, 1994; Yokota et al., 1999; Tominaga et al., 2012). The coiled-coil domain facilitates dimerization (Li and Nebenführ, 2008), and the globular tail functions as the cargo-binding domain (Li and Nebenführ, 2007). Class VIII myosins also contain an N-terminal extension, MyTH8 (for myosin tail homology8; Mühlhausen and Kollmar, 2013), and class XI myosins contain a dilute domain in the C-terminal globular tail (Kinkema and Schiefelbein, 1994; Odronitz and Kollmar, 2007; Sebé-Pedrós et al., 2014). Recently, Mühlhausen and Kollmar (2013) proposed a new nomenclature for plant myosins based on a comprehensive phylogenetic analysis of all known plant myosins that clearly identifies paralogs and makes interspecies comparisons easier (Madison and Nebenführ, 2013).

The localization of class VIII myosins, as determined by immunolocalization and the expression of fluorescently labeled full-length or tail constructs, has implicated these myosins in cell-to-cell communication, cell division, and endocytosis in angiosperms and moss (Reichelt et al., 1999; Van Damme et al., 2004; Avisar et al., 2008; Golomb et al., 2008; Sattarzadeh et al., 2008; Yuan et al., 2011; Haraguchi et al., 2014; Wu and Bezanilla, 2014). On the other hand, class XI myosin mutants have been studied extensively in Arabidopsis (*Arabidopsis thaliana*), which revealed roles for class XI myosins in cell expansion and organelle motility (Ojangu et al., 2007, 2012; Peremyslov et al., 2008, 2010; Prokhnevsky et al., 2008; Park and Nebenführ, 2013). Very few studies have examined the reproductive tissues of class XI myosin mutants. In rice (*Oryza sativa*), one myosin XI was shown to be required for normal pollen development under short-day conditions (Jiang et al., 2007). In Arabidopsis, class XI myosins are required for stigmatic papillae elongation, which is necessary for normal fertility (Ojangu et al., 2012). Even though pollen tubes of myosin XI mutants have not been examined, the tip growth of another tip-growing plant cell has been thoroughly examined in myosin mutants. Root hairs are tubular outgrowths of root epidermal cells that function to increase the surface area of the root for water and nutrient uptake. Two myosin XI mutants have shorter root hairs, of which the *myo11e1* (*xik*; myosin XI K) mutation has been shown to be associated with a slower root hair growth rate and reduced actin dynamics compared with the wild type (Ojangu et al., 2007; Peremyslov et al., 2008; Park and Nebenführ, 2013). Higher order mutants have a further reduction in root hair growth and have altered actin organization (Prokhnevsky et al., 2008; Peremyslov et al., 2010). Disruption of actin organization was also observed in myosin XI mutants of the moss *Physcomitrella patens* (Vidali et al., 2010), where these motors appear to coordinate the formation of actin filaments in the apical dome of the tip-growing protonemal cells (Furt et al., 2013). Interestingly, organelle movements in *P. patens* are much slower than in angiosperms and do not seem to depend on myosin motors (Furt et al., 2012).

The function of myosins in pollen tubes is currently not known, although it is generally assumed that they are responsible for the prominent cytoplasmic streaming observed in these cells by associating with organelle surfaces (Kohno and Shimmen, 1988; Shimmen, 2007). Myosin from lily (*Lilium longiflorum*) pollen tubes was isolated biochemically and shown to move actin filaments with a speed of about 8 μm s^{-1} (Yokota and Shimmen, 1994) in a calcium-dependent manner (Yokota et al., 1999). Antibodies against this myosin labeled small structures in both the tip region and along the shank (Yokota et al., 1995), consistent with the proposed role of this motor in moving secretory vesicles to the apex.

In Arabidopsis, six of 13 myosin XI genes are highly expressed in pollen: *Myo11A1* (*XIA*), *Myo11A2* (*XID*), *Myo11B1* (*XIB*), *Myo11C1* (*XIC*), *Myo11C2* (*XIE*), and *Myo11D* (*XIJ*; Peremyslov et al., 2011; Sparkes, 2011). The original gene names (Reddy and Day, 2001) are given in parentheses. *Myo11D* is the only short-tailed myosin XI in Arabidopsis (Mühlhausen and Kollmar, 2013) and lacks the typical myosin XI globular tail involved in cargo binding (Li and Nebenführ, 2007). The remaining genes have the same domain architecture as the conventional class XI myosins that have been shown to be involved in the elongation of trichomes, stigmatic papillae, and root hairs (Ojangu et al., 2007, 2012; Peremyslov et al., 2008, 2010; Prokhnevsky et al., 2008; Park and Nebenführ, 2013). Therefore, we predicted that these five pollen-expressed, conventional class XI myosins are required for the rapid elongation of pollen tubes. In this study, we examined transfer DNA (T-DNA) insertion mutants of *Myo11A1*, *Myo11A2*, *Myo11B1*, *Myo11C1*, and *Myo11C2* for defects in fertility and pollen tube growth. Organelle motility and actin organization were also examined in *myo11c1 myo11c2* pollen tubes.

RESULTS

Pollen Myosins Are Required for Normal Seed Set

Homozygous T-DNA insertion mutants of *Myo11A1* (At1g04600), *Myo11A2* (At2g33240), *Myo11B1* (At1g04160), *Myo11C1* (At1g08730), and *Myo11C2* (At1g54560) were isolated and confirmed to be knockout mutants by reverse transcription (RT)-PCR (see "Materials and Methods"). Of the pollen myosins, Myo11C1 and Myo11C2 are most similar to each other, with 90.3% identity at the amino acid level. Myo11A1 and Myo11A2 are also very similar to each other, with 77.9% identity (Supplemental Table S1). Therefore, we hypothesized that Myo11C1 and Myo11C2 would

have at least partial overlapping functions and that Myo11A1 and Myo11A2 would also be partially redundant. Thus, *myo11c1 myo11c2* and *myo11a1 myo11a2* double homozygous mutants were generated.

Pollen myosin mutant plants developed normally without obvious phenotypes and also produced seeds, suggesting that the pollen myosin mutants tested here were able to produce viable pollen. We reasoned that if pollen myosin mutants had defects in pollen tube growth, we should be able to detect a reduction in overall fertility, as has been observed for other pollen mutants (Boavida et al., 2009; Zhu et al., 2013). Therefore, the average number of seeds in 10-mm-long siliques from several plants was determined for the wild type (Columbia-0 [Col-0]), *myo11a1-1*, *myo11a1-2*, and *myo11b1-1* (Fig. 1A). Both *myo11a1* mutants had significantly fewer seeds per silique than the wild type ($P < 0.01$). *myo11b1-1* had slightly fewer seeds than the wild type, but this number was not statistically different from the wild type.

To further examine the reduced seed-set phenotype in *myo11a1* mutants, every unopened silique on inflorescences initiating from the rosette was collected from one wild-type, two *myo11a1-1*, and three *myo11a1-2* plants. Collecting mature siliques of all lengths allowed for a more detailed analysis of seed-set differences between the wild type and mutants than the previous experiment. The number of seeds per silique positively correlated with silique length for all three genotypes ($r^2 > 0.75$; Fig. 1D). Instead of comparing the average number of seeds at each length, we developed a method for combining all of the data into one comparison of the number of seeds per 1 mm of silique. To adjust for silique length, the average length of unfertilized siliques (4.1 mm; Vivian-Smith et al., 2001) was subtracted from each silique length, and the corrected length values were used to divide the seed count values. The new, scaled seeds mm^{-1} values no longer correlated with silique length ($r^2 < 0.02$; Fig. 1E). Importantly, this approach reduced the coefficient of variation from over 26% for the seeds-per-silique data to less than 16% for the seeds mm^{-1} data, thus increasing our statistical power. In this experiment, the *myo11a1* mutants had significantly fewer seeds mm^{-1} than the wild type ($P < 0.0001$; Fig. 1B). This difference could not be detected with simple comparison of the number of seeds per silique ($P > 0.13$). Interestingly, average silique length did not vary between the wild type and the *myo11a1* mutants (Fig. 1C), suggesting that *Myo11A1* is required for seed set but not silique length. Thus, our method of measuring seeds mm^{-1} appears to be sensitive enough to detect small differences in seed set that are not perceptible with visual inspection.

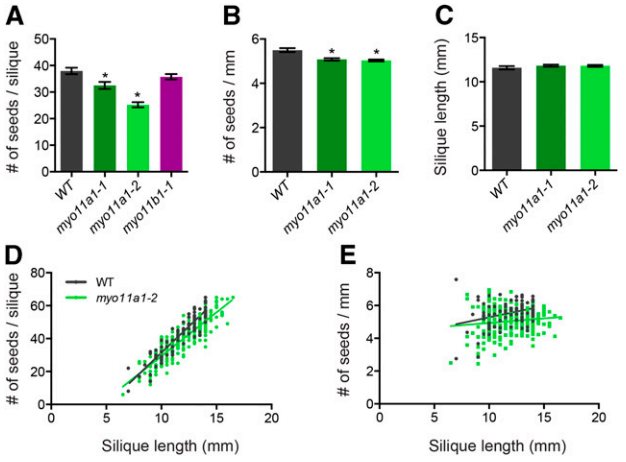

Figure 1. *myo11a1* mutants had reduced seed set. A, Ten-millimeter-long siliques were collected from at least five wild-type (WT), *myo11a1-1*, *myo11a1-2*, and *myo11b1-1* plants, and the number of seeds in each silique were manually counted (mean ± SE; $n = 50$; *, $P < 0.01$). *myo11a1* mutants had significantly fewer seeds per silique than the wild type. B to E, All unopened siliques were collected from one wild-type, two *myo11a1-1*, and three *myo11a1-2* plants ($n = 84$, 178, and 281). B, *myo11a1* mutants had significantly fewer seeds mm^{-1} than the wild type (mean ± SE; *, $P < 0.0001$). C, There was no difference between wild-type and mutant silique lengths. D, Silique length and the number of seeds per silique had a positive correlation for all three genotypes (only the wild type and *myo11a1-2* are shown to reduce clutter). E, Seeds mm^{-1} were calculated by dividing the number of seeds by (length – 4.1); 4.1 mm was the mean average silique length for emasculated wild-type flowers (Vivian-Smith et al., 2001). Note the lack of correlation between seeds mm^{-1} and silique length (only the wild type and *myo11a1-2* are shown).

With this new method for analyzing seed-set data, all single and double mutants for *Myo11A1*, *Myo11A2*, *Myo11C1*, and *Myo11C2* were grown to collect siliques for analysis. In these experiments, unopened and opened siliques were collected from the primary inflorescences of multiple plants. Plants were grown in four separate experiments, and mutants were always compared with the wild-type control from their own experiment (Fig. 2). The most striking phenotype observed was for *myo11c1 myo11c2*. All three allele combinations for *myo11c1 myo11c2* double mutants had shorter siliques and fewer seeds mm^{-1} than the wild type (Fig. 2; $P < 0.05$). These mutants were also the only ones with visibly fewer seeds per silique than the wild type (Fig. 3). Gaps were frequently observed at the bottom of the *myo11c1 myo11c2* siliques (Fig. 3B), suggesting that there was a defect in *myo11c1 myo11c2* pollen tube growth (Boavida et al., 2009; Zhu et al., 2013) rather than a problem with the female gametophyte or general seed development. These defects were not observed in either of the *myo11c1* or *myo11c2* single mutant alleles, suggesting that Myo11C1 and Myo11C2 function redundantly in their role in fertility. Consistent differences from the wild type were not detected for mutants of *Myo11A2* (Fig. 2). Curiously, the reduced seed set of *myo11a1* mutants observed previously could not be confirmed in this set of experiments (compare Figs. 1B and 2A). This may have been the result of reduced sample size or subtle changes in growth conditions, since we also observed variable seed set for wild-type plants from different experiments when measured as seeds mm^{-1} (Fig. 2).

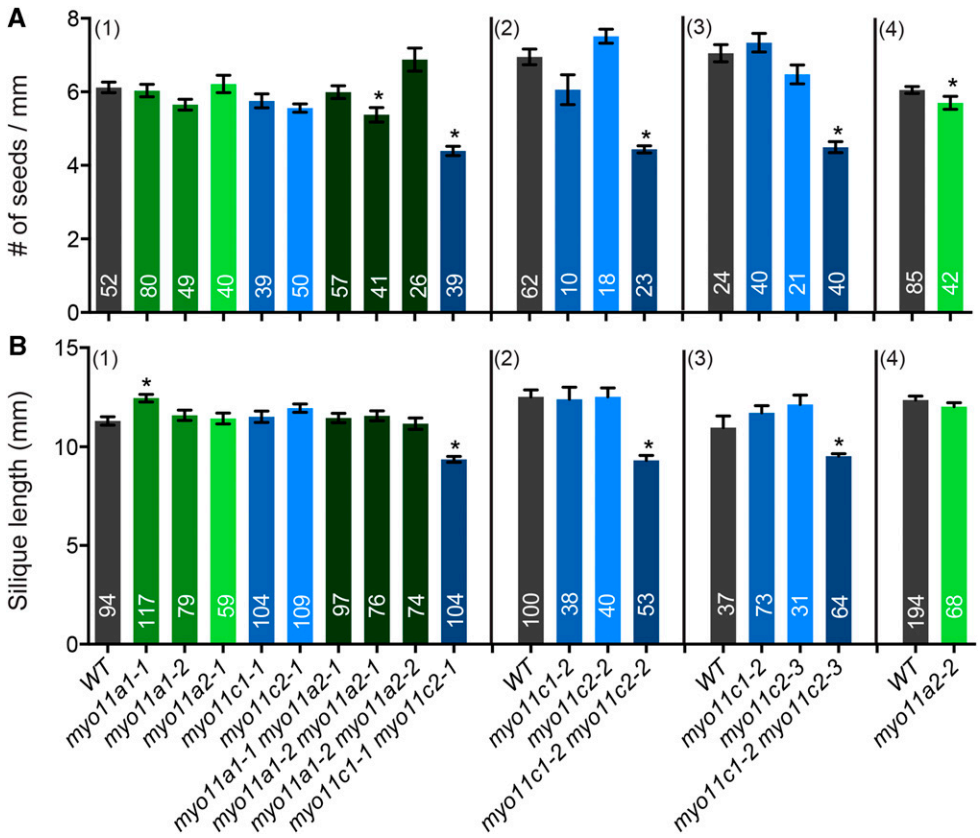

Figure 2. *myo11c1 myo11c2* mutants had shorter siliques with fewer seeds. Mature siliques were collected in four separate experiments (1–4), and the average number of seeds mm^{-1} (A) and silique lengths (B) of the mutants were compared with the wild type (WT) of that experiment (mean ± SE; *, $P < 0.05$). All three allele combinations of *myo11c1 myo11c2* had shorter siliques and fewer seeds mm^{-1} than the wild type. Numbers in the columns indicate the number of siliques analyzed that were collected from between one and five plants per genotype.

Some Myosin Mutants Have Reduced Pollen Fitness

The previous experiments demonstrated that some pollen myosins are required for optimal fertilization, suggesting that mutant alleles should display segregation distortion. This was observed for the *myo11c1 myo11c2* double mutant (Table I). When generating all three allele combinations for *myo11c1 myo11c2*, significantly fewer double homozygous mutants were obtained in the F2 generation than expected ($\chi^2 > 4.8$, $P < 0.05$; Table I). In fact, two of the allele combinations were only brought to homozygosity in the F3 generation. *Myo11C1* and *Myo11C2* are more than 17 Mb apart on different arms of chromosome 1 (The Arabidopsis Information Resource [TAIR] 10) and are expected to be unlinked (Koornneef et al., 1983). Therefore, the segregation distortion likely was caused by a defect in the male gametophyte, the female gametophyte, or during embryo development. Given that *Myo11C1* and *Myo11C2* are primarily expressed in pollen based on microarray experiments (Peremyslov et al., 2011; Sparkes, 2011) and promoter-reporter fusion constructs (E. Park and A. Nebenführ, unpublished data), a pollen defect is the most probable explanation. Segregation distortion was not observed for any of the allele combinations for *myo11a1 myo11a2* ($\chi^2 < 1.8$, $P > 0.05$; Table I).

Given the absence of effects on seed set for single mutants, we predicted that a large population of offspring would have to be analyzed in order to detect weak effects on allele segregation. We took advantage of fluorescently tagged lines (FTLs) that had marker genes inserted in close proximity to the wild-type alleles of *Myo11A1* and *Myo11B1* on chromosome 1 (Francis et al., 2007; Roy et al., 2011). To detect the differential fertilization success of pollen with different genotypes, we tested for potential segregation distortion in offspring from heterozygous plants carrying both fluorescently labeled wild-type (WT^+) and unlabeled mutant alleles. Pollen carrying the *myo11b1-1* allele had significantly reduced fertilization success compared with *Myo11B1* pollen ($P = 0.011$), while the *myo11a1* mutants were similar to WT^+ (Table II). It should be noted that the defect in *myo11b1-1* is small, resulting in a male transmission efficiency of about 0.8.

Myo11C1 and *Myo11C2* Function Redundantly to Sustain Normal Pollen Tube Growth in Vitro

To directly examine the role of myosins in pollen tube growth, pollen from all single and double mutants were grown in vitro along with WT* as a control. WT* pollen expressed a yellow fluorescent protein (YFP)-peroxisome marker and allowed us to control for experimental variation from slide to slide. Three hours after setup, pollen tube growth rates and lengths were

Figure 3. *myo11c1 myo11c2* mutants lacked seeds in the bottom half of siliques. *myo11c1 myo11c2* mutants (B) had fewer seeds per silique than the wild type (A). There were fewer seeds in the bottom half of *myo11c1 myo11c2* siliques. Bar = 1 mm.

measured, adjusted to WT*, and compared with the wild type (Fig. 4). Mutants lacking single myosin genes had growth rates similar to the wild type, although both *myo11b1* alleles, two of the *myo11a1 myo11a2* allele combinations, and all three *myo11c1 myo11c2* allele combinations showed somewhat slower growth. The only statistically significant difference in growth rate was found for the *myo11c1-1 myo11c2-1* double mutant, indicating that these two genes are most important for pollen tube growth. Overall, growth rates varied widely within all genotypes (Supplemental Fig. S1A), making the detection of significant differences from the wild type difficult. Variation of pollen tube lengths at this time point was even larger, often ranging from 15 μm to more than 800 μm for a given genotype (Supplemental Fig. S1B). This large divergence may have resulted not only from different growth rates but also from variable germination times of individual pollen grains, although we did not detect any delay in germination times for any of the myosin mutant genotypes. Despite this large variation, *myo11c1 myo11c2* pollen tubes were found to be significantly shorter than wild-type tubes for all three allele combinations (Supplemental Fig. S1B), again suggesting that the *Myo11C1* and *Myo11C2* genes together play an important role in pollen tube elongation.

Double Mutants Have Slower Pollen Tube Growth Rates in Vivo

To determine whether myosin mutants had defects in pollen tube growth under in vivo conditions, male-sterile (*ms1*) plants were pollinated with one of the following genotypes: wild type, *myo11a1-1 myo11a2-1*, *myo11b1-1*, or *myo11c1-1 myo11c2-1*. We tested only one allele or allele combination per genotype, as the previous experiments did not reveal any difference between the different knockout alleles. Pollinated pistils were fixed at various time points, and the pollen tubes were stained with Aniline Blue. For each pistil, the farthest distance traveled by a pollen tube was measured (Supplemental Fig. S2). The distance was measured in a straight line, so the actual path taken by a given pollen tube was considerably longer (Crawford and Yanofsky, 2011). The farthest distance traveled for both double mutant pollen, *myo11a1-1 myo11a2-1* and *myo11c1-1 myo11c2-1*, was significantly shorter than that for wild-type pollen at all four time points ($P < 0.01$; Fig. 5A), with the *myo11c1-1 myo11c2-1* mutant reaching only about 40% of the length of wild-type pollen tubes. Delayed germination of *myo11c1-1 myo11c2-1* pollen was unlikely to have caused the shorter pollen tubes, as pollen from all genotypes had reached the style after 110 min. The trajectories of the mutant pollen tubes also did not appear to be less straight or more meandering than those of the wild type. Extrapolating from the pollen tube lengths at 195 and 360 min after pollination, we calculated average growth rates of 4.1 $\pm$ 1.5 μm min^{-1} for the wild type, 2.3 $\pm$ 1.2 μm min^{-1} for *myo11a1-1 myo11a2-1*, 3.2 $\pm$ 1.3 μm min^{-1} for *myo11b1-1*, and 1.4 $\pm$ 0.8 μm min^{-1} for *myo11c1-1 myo11c2-1* (Fig. 5B), indicating that the two double mutants had

Table I. *Segregation distortion detected while generating the myo11c1 myo11c2 double mutant*

The number of double homozygous mutants obtained from screening the F2 generations is shown. *P* values were derived from χ^2 analysis. Significantly fewer homozygous *myo11c1 myo11c2* double mutants were obtained than expected, while no segregation distortion was observed for the *myo11a1 myo11a2* allele combinations. Double homozygous mutants were obtained in the F3 generation for the lines indicated with asterisks.

Genes	Alleles	No. of Homozygous/No. of Total F2 Screened	Expected	*P*
Myo11A1	*myo11a1-1 myo11a2-1*	3/77	4.8/77	0.36
Myo11A2	*myo11a1-2 myo11a2-1*	1/22	1.4/22	0.71
	myo11a1-2 myo11a2-2	1/53	3.3/53	0.18
Myo11C1	*myo11c1-1 myo11c2-1*	1/101	6.3/101	0.028
Myo11C2	*myo11c1-2 myo11c2-2* *	0/96	6.0/96	0.011
	myo11c1-2 myo11c2-3 *	0/103	6.4/103	0.0088

Table II. *myo11b1 pollen was less fit than wild-type pollen*

The number of offspring resulting from pollination of *ms1* plants with pollen from plants heterozygous for a marker gene near the *Myo11B1* or *Myo11A1* gene is shown. *P* values were based on χ^2 analysis. Pollen carrying the *myo11b1-1* allele had significantly reduced fertilization success compared with WT$^+$, while the *myo11a1* mutants were similar to WT$^+$.

Test Genotype	No. of Test Offspring	No. of WT$^+$ Offspring	*P*
Wild type	670	664	0.87
myo11b1-1	188	241	0.011
Wild type	378	355	0.40
myo11a1-1	271	315	0.069
myo11a1-2	342	349	0.79

significantly slower in vivo pollen tube growth rates than the wild type ($P < 0.001$).

Starting at 195 min postpollination, *myo11b1-1* had shorter pollen tubes than the wild type; however, the length of *myo11b1-1* pollen was not always statistically different from that of wild-type pollen tubes (Fig. 5A), and the growth rate was also not significantly different between 195 and 360 min (Fig. 5B). This result was consistent with *myo11b1-1* pollen being slightly less fit than wild-type pollen in the pollen competition experiment (Table II).

myo11c1 myo11c2 Pollen Tubes Have Reduced Organelle Motility

Single and higher order myosin XI mutants have reduced organelle motility in vegetative tissues (Peremyslov et al., 2008, 2010; Prokhnevsky et al., 2008; Ueda et al., 2010). Furthermore, drug treatments that disrupt actin filaments have been shown to inhibit organelle movements in pollen tubes (Mascarenhas and Lafountain, 1972; Heslop-Harrison and Heslop-Harrison, 1989; Vidali et al., 2001). Hence, we hypothesized that pollen myosin mutants would also have reduced organelle motility. Since *myo11c1 myo11c2* pollen tubes exhibited the strongest growth defects, peroxisome and Golgi stack movements were examined in wild-type and *myo11c1 myo11c2* pollen tubes.

Wild-type or *myo11c1-1 myo11c2-1* pollen tubes stably expressing either a YFP-peroxisome or YFP-Golgi marker were grown in vitro and examined using wide-field epifluorescence microscopy. *myo11c1-1 myo11c2-1* pollen tubes had visually reduced peroxisome and Golgi stack movements compared with wild-type pollen tubes (Fig. 6A; Supplemental Movies S1 and S2). At least nine independent, 2-min time-lapse image sequences with 0.5-s intervals between images were captured for each treatment. Organelles were detected and tracked automatically using the Particle Tracker plug-in (Sbalzarini and Koumoutsakos, 2005) for ImageJ. The cumulative frequency distribution of velocities was plotted for all measurements from individual pollen tubes. The frequency distribution of Golgi stack and peroxisome velocities varied greatly between pollen tubes of the same genotype (Fig. 6, B and C). Despite this variation from cell to cell, the results from wild-type and *myo11c1-1 myo11c2-1* pollen tubes were clearly separated (Fig. 6, B and C). Velocities were then combined by genotype, and the cumulative frequency distribution of velocities between the wild type and *myo11c1-1 myo11c2-1* were significantly different from each other ($P < 0.0001$; Fig. 6, D and E).

After examining the tracking results in detail, it was apparent that the automated tracking program made some errors due to the high velocity and high density of the organelles in pollen tubes. Occasionally, an organelle in one frame would be incorrectly linked to a different organelle in the next frame, as has been described previously (Chenouard et al., 2014). This error in linking often resulted in false high-velocity measurements that affected the cumulative frequency distributions (Fig. 6). Nevertheless, the clear difference in velocity distribution detected by automatic tracking (Fig. 6) is still valid, as the algorithm made few mistakes at slower velocities (less than 1 $\mu m\ s^{-1}$) that represent 64% to 98% of all measurements. To gain a more reliable understanding of the quantitative differences of fast organelle movements, we manually measured the velocities of organelles that were visually identified as moving very fast. For wild-type pollen tubes, the maximum speeds for peroxisomes and Golgi stacks measured by manual tracking were 6.6 and 5.9 $\mu m\ s^{-1}$, respectively

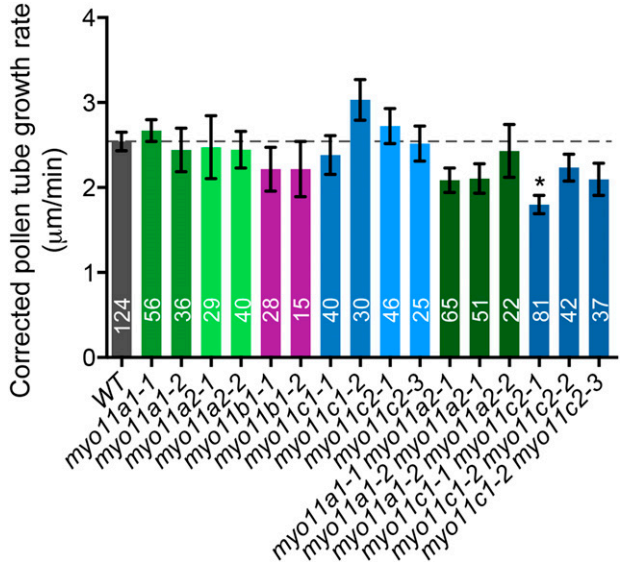

Figure 4. Some mutants had reduced pollen tube growth rates in vitro. Three hours after incubation, growth rates for wild-type (WT) and mutant pollen were measured and corrected based on the control (WT*) included on each slide. Each genotype was tested between two and 10 times, and all replicates with the same genotypes were combined (mean ± SE; *, $P < 0.05$). The pollen tubes from *myo11b1* and from double mutants tended to grow slower than wild-type pollen tubes, but only one allele combination of *myo11c1 myo11c2* had a statistically significant reduction in growth rate. Sample sizes (number of pollen tubes) are given in the columns.

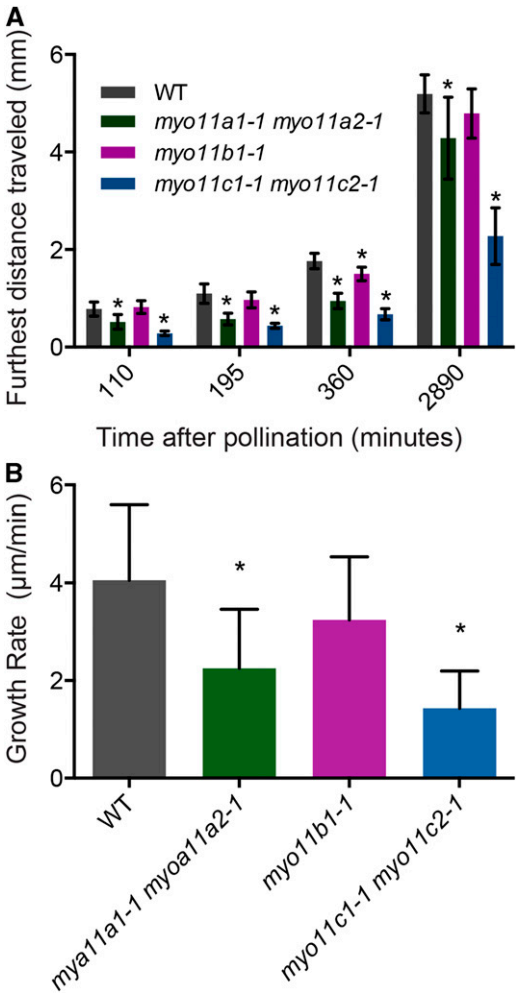

Figure 5. Some myosin mutants had slower pollen tube growth rates in vivo. A, Wild-type (WT), *myo11a1-1 myo11a2-1*, *myo11b1-1*, or *myo11c1-1 myo11c2-1* pollen was used to pollinate *ms1* plants. Pollinated pistils were removed, fixed, and stained with Aniline Blue at the indicated time points after pollination. For each pistil, the farthest distance traveled by a pollen tube was measured (mean ± SD; $n = 4–23$; *, $P < 0.01$). Pollen tubes of *myo11a1-1 myo11a2-1* and particularly of *myo11c1-1 myo11c2-1* mutants grew more slowly than wild-type pollen, while pollen tubes of *myo11b1-1* showed only a small difference from wild-type pollen. B, Average pollen tube growth rates between 195 and 360 min after pollination. Growth rates and expected SD values were calculated from the change in pollen tube lengths in A (*, $P < 0.001$).

(Supplemental Fig. S3). For *myo11c1-1 myo11c2-1* pollen tubes, the maximum speeds measured for peroxisomes and Golgi stacks were 1.8 and 3.3 μm s^{-1}, respectively (Supplemental Fig. S3). These maximal velocities are considerably slower than those determined by automatic tracking, particularly for the mutant pollen tubes, but they still reflect a drastic reduction in movement speeds in *myo11c1 myo11c2* mutant pollen tubes. Similarly, the percentage of movement steps above 1 μm s^{-1} measured in these fast-moving organelles decreased from more than 50% in the wild type to less than 10% in the mutant (Supplemental Fig. S3), demonstrating that Myo11C1 and Myo11C2 are required for rapid movements of both peroxisomes and Golgi stacks.

In order to determine whether organelle movements were also affected in other myosin mutants, we analyzed time-lapse videos of differential interference contrast (DIC) images of the different genotypes (Supplemental Fig. S4A; Supplemental Movie S3). The velocities of individual particles of unknown identity were tracked in kymographs (Supplemental Fig. S4B) with a strong bias to fast-moving particles, as these were most likely to reveal defects in myosin-dependent movements. Interestingly, we did not detect significant differences in movement speeds between any of the mutants and the wild type except for *myo11c1 myo11c2* (Supplemental Fig. S4C). This suggests that loss of myosin isoforms other than Myo11C has only minor effects on organelle movements in pollen tubes.

Movement and Tip Accumulation of YFP-RabA4d Vesicles Is Normal in *myo11c1 myo11c2* Pollen Tubes

The small GTPase RabA4d associates with vesicles that accumulate dynamically and are dependent on actin filaments at the tip of growing pollen tubes (Lee et al., 2008). Disruption of *RabA4d* leads to reduced in vitro pollen tube growth rates as well as reduced pollen transmission and in vivo growth defects (Szumlanski and Nielsen, 2009), demonstrating that YFP-RabA4d-decorated vesicles are important for pollen tube growth. In tobacco (*Nicotiana tabacum*) pollen tubes, oscillations of YFP-RabA4d accumulation at the tip precede growth bursts by about 10 s (Lee et al., 2008), suggesting a direct link between RabA4d vesicles and pollen tube growth.

In order to test whether the reduced growth of *myo11c1 myo11c2* pollen tubes correlated with a reduced accumulation of RabA4d-labeled vesicles at the tip, we introduced a *YFP-RabA4d* construct under the control of a pollen-specific promoter into both wild-type and double mutant plants. Unexpectedly, accumulation of the marker at the tip was similar in the two genotypes (Fig. 7A), suggesting that Myo11C1 and Myo11C2 are not required for normal vesicle accumulation. Time-lapse observations of growing pollen tubes confirmed previous reports that this tip accumulation is dynamic (Lee et al., 2008; Szumlanski and Nielsen, 2009) and involves continuous delivery of YFP-RabA4d vesicles in the periphery of the tube and concomitant removal near the center (Supplemental Movie S4). YFP-RabA4d accumulation at the tip was always maintained in growing *myo11c1 myo11c2* pollen tubes, although the streaming pattern within the tip region sometimes seemed disordered. To determine whether the velocity of YFP-RabA4d vesicles was affected in the *myo11c1 myo11c2* mutant, we analyzed their movements in time-lapse images. The high density of the vesicles combined with their low signal-to-noise ratio

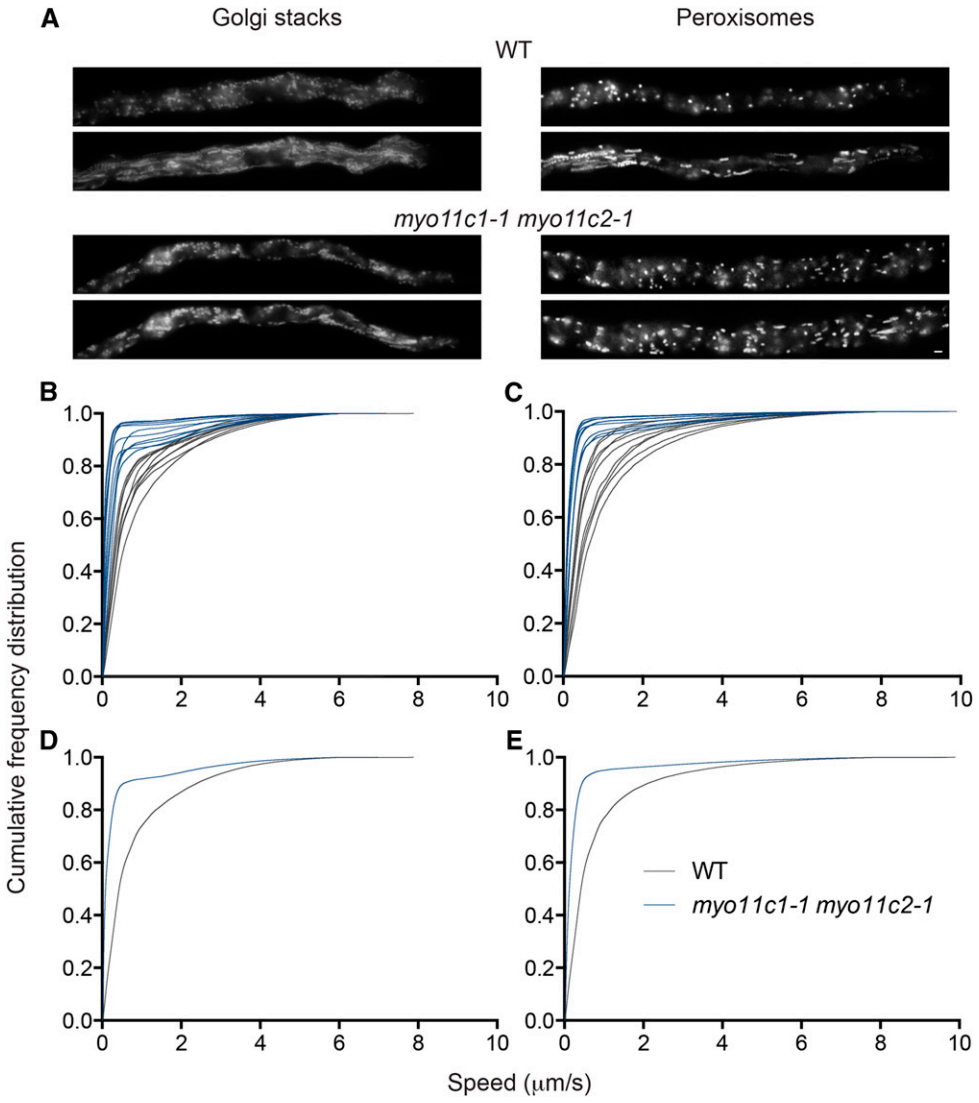

Figure 6. Peroxisomes and Golgi stacks had reduced motility in *myo11c1 myo11c2* pollen tubes. Wild-type (WT) and *myo11c1-1 myo11c2-1* pollen tubes expressing either a YFP-Golgi marker (left column) or a YFP-peroxisome marker (right column) were imaged for 2 min at 0.5-s intervals. A, For each genotype, the first frame (top) was compared with the first 20 frames, representing 10 s, merged (bottom). *myo11c1-1 myo11c2-1* pollen tubes had visually reduced Golgi stack (left) and peroxisome (right) movements than wild-type pollen tubes. Bar = 2 μm. B to E, Organelles were detected and velocities were measured for each frame by an automated algorithm. Speed measurements were combined for each pollen tube (B and C) and by genotype (D and E) and plotted as cumulative frequency distribution graphs. Golgi stacks and peroxisomes moved more slowly in *myo11c1 myo11c2* pollen tubes (blue lines) than in wild-type pollen tubes (black lines).

precluded direct tracking of individual vesicles. Therefore, we used kymographs to analyze their retrograde movements in the center of pollen tubes (Fig. 7B). Interestingly, traces of individual YFP-RabA4d spots in the kymographs seemed to follow similar trajectories in both wild-type and double mutant pollen tubes. Measurement of the angle formed by typical traces (n = 174 per genotype) allowed us to determine their velocities. The maximal speeds observed in 17 wild-type and 20 mutant pollen tubes were not significantly different from each other (Fig. 7C), while average velocities were only slightly slower in the mutant (1.3 ± 0.57 μm s^{-1} for the wild type and 1.1 ± 0.58 μm s^{-1} for *myo11c1 myo11c2*). These results suggest that, contrary to Golgi stack and peroxisome movements, Myo11C function is not required for the movement and tip accumulation of RabA4d vesicles. Furthermore, we did not detect any correlation between pollen tube growth rates and movement speeds of YFP-RabA4d vesicles (data not shown).

Actin Filaments Are Less Ordered in *myo11c1 myo11c2* Pollen Tubes

In vegetative tissues, it has been shown that loss of myosin motors not only affects organelle movements but also the organization and dynamics of actin filaments (Peremyslov et al., 2010; Ueda et al., 2010; Park and Nebenführ, 2013). To test whether a similar effect might occur in *myo11c1 myo11c2* pollen tubes, we expressed the YFP-FABD2 (for fimbrin actin binding domain2) actin marker (Voigt et al., 2005; Park and Nebenführ, 2013) under the control of a pollen-specific promoter in both the wild type and *myo11c1 myo11c2* and visualized the actin filaments present in the shank of the pollen tubes. Visual inspection of the maximal intensity projections showing all actin filaments in a cell revealed a clear difference in organization between the wild type and the mutant (Fig. 8A). Whereas actin filaments in wild-type cells were often found in thick bundles running along the long axis of the pollen tube,

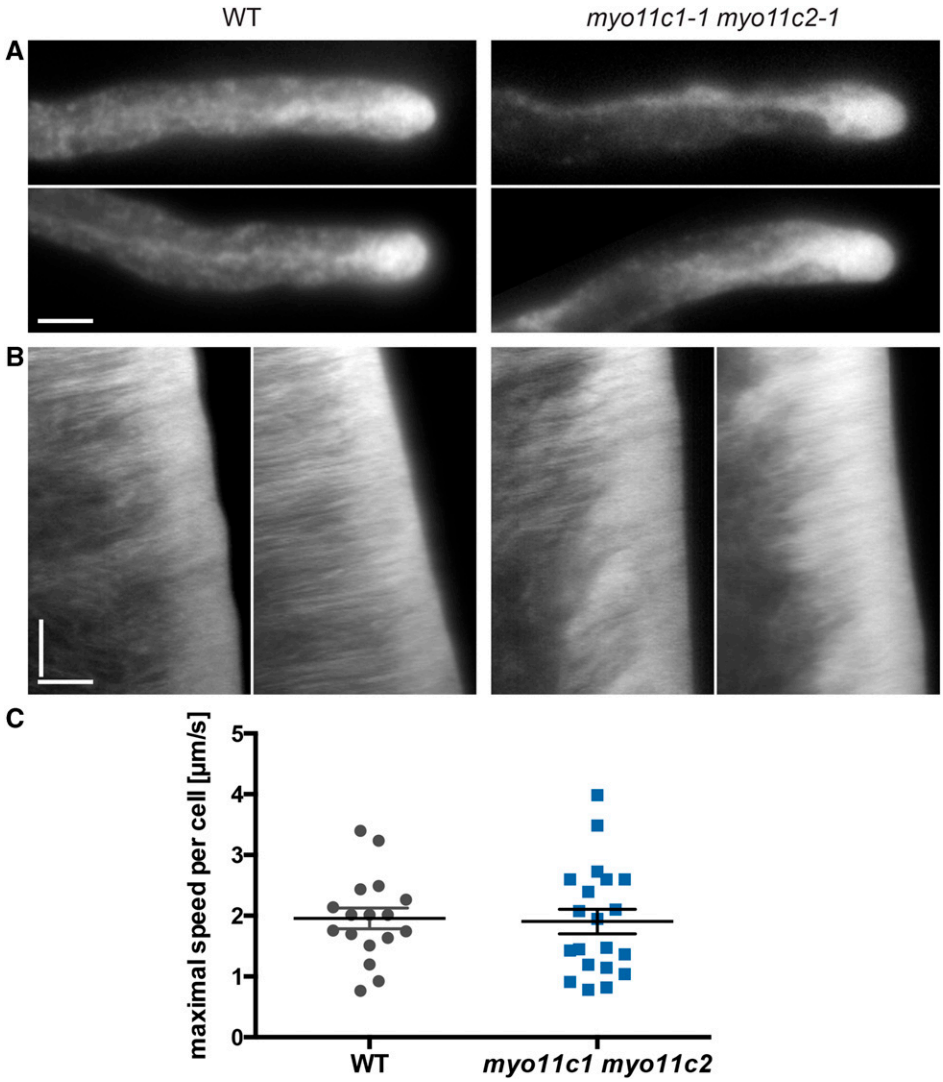

Figure 7. YFP-RabA4d vesicles accumulated and moved normally in *myo11c1 myo11c2* pollen tubes. A, Distribution of YFP-RabA4d signal near the midplane of two wild-type (WT; left) and two *myo11c1-1 myo11c2-1* (right) pollen tubes. The distribution of YFP-RabA4d vesicles appeared qualitatively similar between genotypes. Bar = 5 μm. B, Kymographs illustrating YFP-RabA4d movement near the midline of pollen tubes in A. The *y* axis represents time (bar = 20 s), and the *x* axis represents the position along the tube (bar = 5 μm). Lines slanting to the left indicate the movement of vesicles away from the tip. C, Maximal speed of YFP-RabA4d vesicles in wild-type (gray) and *myo11c1-1 myo11c2-1* (blue) pollen tubes. Horizontal lines indicate means and SE.

we saw less bundling, more branching, and many different orientations of actin filaments in *myo11c1 myo11c2* pollen tubes.

In order to quantify these different organizations, we developed an algorithm that automatically identifies actin filaments in fluorescence images (see "Materials and Methods"). Given these simplified actin images (Supplemental Fig. S5B), we first measured the parallelness of the filaments (Ueda et al., 2010), which compares the relative frequencies of horizontal and vertical pixel pairs as well as up-diagonal and down-diagonal pixel pairs. This analysis revealed a reduced level of parallelness in mutant pollen tubes (0.66 $\pm$ 0.09 in *myo11c1 myo11c2* versus 0.78 $\pm$ 0.08 in the wild type; $P < 0.01$). Closer inspection of the images revealed that this approach was not ideal for those pollen tubes that showed significant curvature within the image, since parallelness is based on pixel pair orientation only relative to the image, not relative to the cell axis. Therefore, we developed a second algorithm that measures the deviation of actin filament angles from the midline of the cell (see "Materials and Methods"; Supplemental Fig. S5C). The average angle calculated in this way was always close to 0° (data not shown), suggesting that filaments deviating to the left or right of the long axis of the cell were present in roughly equal numbers. In contrast, the variation around this mean angle differed substantially between different pollen tubes with visibly different levels of organization. To capture this variation, we define the parameter orderliness as the reciprocal of the SD around the mean angle between actin filaments and the cell midline (see "Materials and Methods"). As expected, the orderliness parameter of a given cell does not always match its parallelness parameter. Nevertheless, the average orderliness of actin filaments in *myo11c1 myo11c2* pollen tubes (0.043 $\pm$ 0.009) was significantly lower than that of wild-type cells (0.058 $\pm$ 0.015; $P < 0.001$). Thus, using both parallelness and orderliness measures, we found that actin filaments are less organized in *myo11c1 myo11c2* mutant pollen

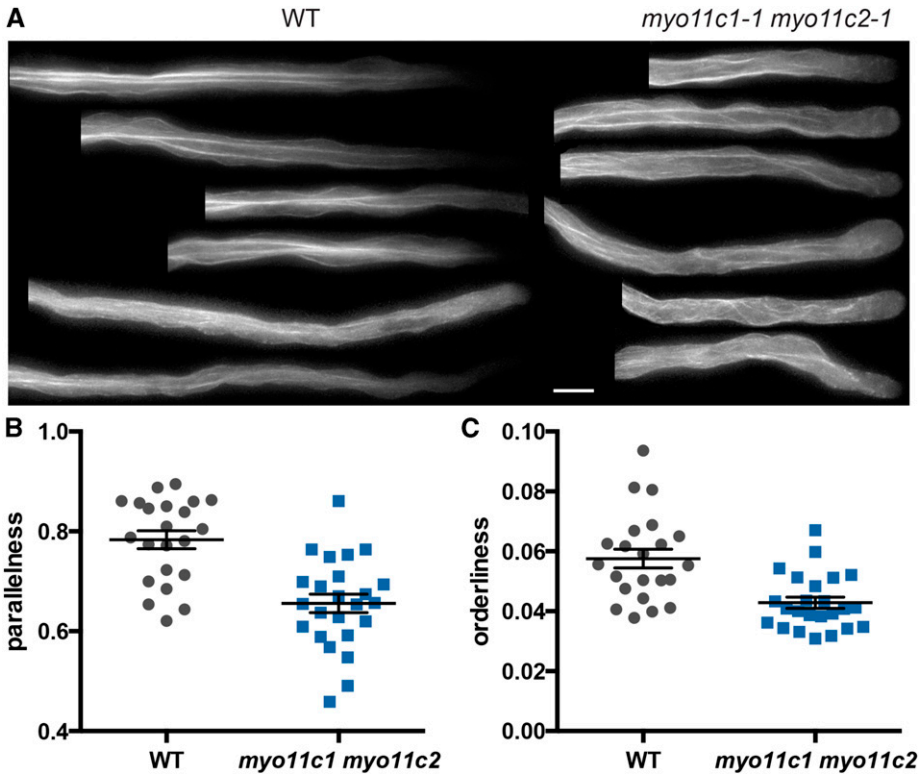

Figure 8. Actin filaments are more disordered in *myo11c1 myo11c2* pollen tubes. A, Organization of YFP-FABD2-labeled actin filaments in six representative wild-type (WT; left) and *myo11c1-1 myo11c2-1* (right) pollen tubes. Images show maximal intensity projections of images taken at several focal planes. Bar = 10 μm. B, Actin filaments are less parallel to each other in *myo11c1-1 myo11c2-1* (blue) than in wild-type (gray) pollen tubes ($P < 0.001$). Horizontal lines indicate means and SE. C, Actin filaments in *myo11c1-1 myo11c2-1* pollen tubes (blue) show less orderliness ($P < 0.001$) than those of the wild type (gray). Orderliness is a measure for the variability of actin filament orientation within a pollen tube. Horizontal lines indicate means and SE.

tubes than in the wild type, suggesting that these myosin isoforms are required for normal actin organization.

DISCUSSION

Pollen tubes display prominent cytoplasmic streaming, and it has been assumed for many years that these intracellular movements are necessary for the tip accumulation of secretory vesicles that drive pollen tube growth. Until now, no direct experimental approach existed that allowed a direct assessment of this conjecture. With the availability of T-DNA insertion mutants in Arabidopsis, the effect of reduced cytoplasmic streaming, due to the loss of myosin motors, on pollen tube growth and reproduction could now be examined. Our results support the model that pollen myosins are necessary for rapid pollen tube growth, which in turn is required for normal fertility. Curiously, we did not detect a significant change in vesicle accumulation at the tip of slow-growing pollen tubes lacking a subset of myosins. This suggests that other factors, such as organelle movements in the shank or actin organization, become limiting for growth in these mutants. At the same time, however, our results demonstrate a functional specialization of myosin motors in pollen tubes.

In order to determine the biological function(s) of pollen-specific myosin motors, we utilized five different experimental approaches that measure different aspects of reproduction. Seed-set analysis measures all events contributing to overall fertility, including pollen development, germination, and tube growth as well as fertilization and embryo development. Segregation distortion and pollen competition experiments measure the relative fitness of genotypes, while in vitro and in vivo pollen tube growth experiments directly measure the effect of the mutation on cell expansion. Overall, each of these experiments can provide unique and useful information when trying to determine the role of a particular gene in reproduction. However, each technique does have its advantages and disadvantages. Based on our experience, a simple seed-set analysis is best suited to detect fertilization problems, although weak defects may go undetected. For pollen tube growth, the technically more challenging in vivo method provided clear results with little variation, which simplified interpretation.

Overall, single pollen myosin mutants had either minor or no defects in pollen tube growth and overall fertility. This suggests that each isoform contributes only a little to pollen tube growth or is redundant with the other pollen myosins, as seen with the pairs of close paralogs, *Myo11A1/Myo11A2* and *Myo11C1/Myo11C2*, respectively. *Myo11B1* seems to play a minor role in pollen tube growth, since mutant pollen was slightly less fit and pollen tubes were slightly shorter than in the wild type. All other experiments with *myo11b1* mutants showed either no effect or were inconclusive. These results are consistent with the minor role of *Myo11B1* in root hair elongation (Prokhnevsky et al., 2008). In that case, however, the strong expression of the close paralog, Myo11B2 (MYA2), which is 87% identical to

Myo11B1, may mask the effect of *myo11b1* in root hairs. It is possible that the two Myo11A proteins, which are about 66% identical to Myo11B1 (Supplemental Table S1), may similarly compensate for the loss of Myo11B1 in pollen tubes.

Myo11A1 and Myo11A2 are similar to each other, which may explain the lack of clear phenotypes in single mutants. Both isoforms together are needed for normal growth in vivo, although the pollen tubes usually reached the lowest ovules. As a result, this pollen tube growth defect affects seed set only marginally and also does not coincide with a reduction in cytoplasmic streaming speeds. Contrary to some results in the seed-set analysis, a direct pollen competition experiment revealed no reduced fitness relative to the wild type. The seed set analysis and pollen competition experiment tested different aspects of reproduction. Even though *Myo11A1* is expressed primarily in pollen (Peremyslov et al., 2011; Sparkes, 2011), we cannot formally exclude the possibility that the reduced seed set was a result of a defect in the female gametophyte, sporophytic tissues, or embryo development.

Myo11C1 and Myo11C2 clearly perform redundant functions, presumably because they are more than 90% identical. Of all pollen myosin genes, *Myo11C1* and *Myo11C2* have the strongest influence on pollen tube growth, since we could see an effect on seed set, segregation distortion, in vivo pollen tube growth, and even for some in vitro pollen tube growth experiments. Golgi stack and peroxisome movements in *myo11c1 myo11c2* mutants were drastically reduced, consistent with their strong influence on pollen tube growth. In contrast, movements of RabA4d vesicles were not affected by a loss of Myo11C1 and Myo11C2 motors, and accumulation of these vesicles at the tip also appeared normal. This suggests that other myosins can move RabA4d vesicles in pollen tubes, whereas these other myosin isoforms have only limited effects on the movements of larger organelles such as peroxisomes and Golgi stacks. Thus, our results present strong evidence for functional specialization among pollen myosins. Similar results have been obtained for Myo11E1 (XIK) and Myo11B2 (MYA2) in vegetative tissues. In this case, the movement of endoplasmic reticulum and mitochondria was affected in *myo11e1* (*xik*) but not *myo11b2* (*mya2*) mutants (Peremyslov et al., 2008; Ueda et al., 2010).

Interestingly, *myo11c1 myo11c2* pollen tubes displayed less organized actin filaments in the shank than the wild type. This phenotype is similar to that described for the *myo11b2 myo11e1* (*mya2 xik*) double mutant in cotyledonary petioles (Ueda et al., 2010), suggesting similar functions of these myosin isoforms. It is not clear at this time what this function is, although the phenotype is reminiscent of loss of the actin-bundling protein FIMBRIN5 (Wu et al., 2010; Su et al., 2012). It is conceivable that this change in actin organization is the primary effect of the Myo11C loss that resulted secondarily in the observed reduction of organelle speeds in the mutant. This model is consistent with data showing myosin-dependent actin filament dynamics (Cai et al., 2014) and with results in root epidermal cells, where Golgi stacks move faster along thick actin bundles whereas the same organelles moved more slowly over fine actin networks (Akkerman et al., 2011). Actin as the primary target of myosin function has also been described for the moss *P. patens*, where myosin accumulation precedes that of actin (Furt et al., 2013) and loss of myosin XI activity disrupts actin filaments completely (Vidali et al., 2010). To what extent moss protonemata and pollen tubes can be compared directly is not clear, since organelle movements are likely not myosin dependent in *P. patens* protonemata (Furt et al., 2012). A corollary of the concept of a secondary effect on organelle movements is that the movements of all organelles should be affected by the actin disorganization, which was contradicted by the lack of an effect on the movement of RabA4d vesicles. Alternatively, it is possible that the reduced movement of Golgi stacks and peroxisomes puts different physical

Table III. *Knockout mutants of pollen myosins*

Lines were obtained from the Arabidopsis Biological Resource Center and confirmed to be knockout mutants by RT-PCR. Lines with asterisks were identified previously as knockout mutants (Peremyslov et al., 2008).

Gene	Arabidopsis Genome Initiative No.	Allele	Insertion Line	Insertion Site
Myo11A1	At1g04600	*myo11a1-1*	SALK_086989	Intron
		myo11a1-2	SALK_117717	Exon
Myo11A2	At2g33240	*myo11a2-1*	SAIL_607_G06	Exon
		myo11a2-2	SALK_033198	Intron
Myo11B1	At1g04160	*myo11b1-1*	SALK_113062*	Exon
		myo11b1-2	SALK_016579	Exon
Myo11C1	At1g08730	*myo11c1-1*	SALK_129231C	Exon
		myo11c1-2	SAIL_905_C08	Intron
Myo11C2	At1g54560	*myo11c2-1*	SALK_072023*	Exon
		myo11c2-2	SALK_089338C	Exon
		myo11c2-3	SALK_025293C	Exon

strains on the actin network that then secondarily reorganizes into a finer network. In this model, the smaller size of the RabA4d vesicles might lead to smaller forces during their movement, which would not be sufficient to restore bundling. Finally, it is possible that the two observations of reduced organelle speeds and actin organization are not functionally linked and independent effects of these myosin mutations. It should also be noted that the FABD2 actin marker used in this study fails to label the dense network of fine actin filaments in the subapical region of pollen tubes. Future studies should examine whether the actin organization and dynamics in the tip region of pollen tubes are also affected in *myo11c1 myo11c2* mutants.

Curiously, pollen tubes lacking functional Myo11C motors displayed normal accumulation of RabA4d vesicles at the pollen tube tip, even though their growth rate was significantly reduced. This result seems to contradict previous reports that suggested an important role for RabA4d vesicles in pollen tube growth (Lee et al., 2008; Szumlanski and Nielsen, 2009). This discrepancy suggests that *myo11c1 myo11c2* mutants affect a different aspect of growth than *raba4d* mutants. This conclusion is also supported by the fact that *raba4d* pollen tubes are wider (Szumlanski and Nielsen, 2009) whereas the width of *myo11c1 myo11c2* tubes (5.7 $\pm$ 0.1 μm [mean $\pm$ SE]; $n = 50$) is identical to that of wild-type tubes (5.7 $\pm$ 0.1 μm; $n = 47$). At this time, it is not clear what this other aspect could be, as it is not known which type of vesicle is labeled by YFP-RabA4d or whether there are different classes of secretory vesicles present in pollen tubes. It is also conceivable that the high expression level of YFP-RabA4d masks a more subtle defect in mutant pollen tubes.

CONCLUSION

Our results clearly demonstrate that the activity of class XI myosins is necessary for rapid pollen tube growth; however, the connection between myosin-driven organelle movements and growth remains unclear. Specifically, we found clear defects in organelle movement and actin organization in the shank but no clear effect on the accumulation and movement of vesicles in the tip. In the future, it will be important to further identify whether other subcellular defects are present in mutant pollen tubes, particularly in the subapical and apical regions, in order to elucidate the exact function of each pollen myosin. Analysis of triple and quadruple mutants between different myosin subtypes will also help to determine the degree of overlapping functions between subtypes Myo11A, Myo11B, and Myo11C. Finally, YFP-tagged complementation constructs will also shed light on this dilemma, because the subcellular localization of each pollen myosin could indicate its function.

MATERIALS AND METHODS

Plant Lines and Growth Conditions

Arabidopsis (*Arabidopsis thaliana*) plants were grown in Fafard Super Fine Germinating Mix in 60% humidity at 22°C in 16 h of light and at 20°C in 8 h of dark. Col-0 was used as the wild type. Seeds for *ms1* (Wilson et al., 2001) were kindly provided by Dr. Ravi Palanivelu. T-DNA insertion lines (Alonso et al., 2003) were ordered from the Arabidopsis Biological Resource Center (Table III). The presence of the T-DNA insertion was confirmed by genomic PCR with primers suggested by T-DNA Express (signal.salk.edu/cgi-bin/tdnaexpress), and absence of the full-length transcript encoded by the disrupted gene was confirmed by RT-PCR with primers spanning the insertion site. Col1-0 was used as the wild type.

Constructs and Plant Transformations

The native *Myo11D* promoter, which extended 757 bp upstream of the *Myo11D* start codon and included the first 9 bp of the *Myo11D* coding sequence (21,534,040–21,534,805 of chromosome 3, based on TAIR 10), was used to drive the expression of the organelle markers. The YFP peroxisome marker has been described previously as part of a larger collection of organelle markers (Nelson et al., 2007). The Golgi marker consisted of the first 49 amino acids of soybean (*Glycine max*) α-1,2-mannosidase I fused to YFP (Saint-Jore-Dupas et al., 2006). The vesicle marker was RabA4d fused to the C terminus of YFP. The full-length *RabA4d* coding sequence was amplified from Arabidopsis flower complementary DNA with primers 5′-GCGGATCCATGTCTAATTTGTATGGAGATT ATA-3′ and 5′-CGCTGCAGTTACGATTTGCCGCAACATCC-3′ (restriction sites for cloning are underlined). The three constructs were each moved into the binary plasmid pVKH18 (Batoko et al., 2000). The actin marker YFP-FABD2 was described previously (Park and Nebenführ, 2013) and was moved into the binary plasmid pPZP221 (Hajdukiewicz et al., 1994). All four constructs were transformed into the wild type and *myo11c1-1 myo11c2-1* by the Arabidopsis floral dip method (Weigel and Glazebrook, 2002).

Seeds-per-Silique Analysis

Plants were grown in individual 6-cm circular pots (except for the wild-type and *myo11a2-2* set, with four plants per 8-cm square pots) until maturity, and individual dry siliques were collected. The silique length was measured to an accuracy of 0.5 mm. Unopened siliques were manually opened, and the seeds were counted. Mutants that were statistically different from the wild type were identified by either an ordinary one-way ANOVA with Dunnett's correction for multiple comparisons or a Mann-Whitney unpaired *t* test depending on the number of genotypes using Prism 6 software (GraphPad).

Pollen Competition Experiment

Seeds for FTL 1285 and FTL 2217 were graciously donated by Dr. Greg Copenhaver. FTL 1285 and FTL 2217 are fluorescently tagged lines that have pollen-specific cytoplasmic DsRed2 or AmCyan markers inserted at positions 80,614 or 2,007,280 on chromosome 1, respectively. *Myo11A1* (1,262,123–1,272,376) and *Myo11B1* (1,086,495–1,096,146) are located near these insertion sites on chromosome 1. Positions are based on TAIR 10. The physical distance of the FTL markers from the myosin genes translates into a genetic distance of approximately 2 to 3 centimorgans, which results in an underestimation of a possible mutant defect by less than 1% and, therefore, has only a very small effect on the outcome of the experiment.

The wild type and *myo11b1-1* were each crossed to FTL 1285, and the wild type, *myo11a1-1*, and *myo11a1-2* were each crossed to FTL 2217. Pollen from the heterozygous F1 plants carried either the unlabeled mutant (or wild-type) allele (test pollen) or the labeled wild-type allele (WT^+ pollen). This pollen was used to pollinate *ms1* flowers. Pollen from the resulting offspring was examined using the AxioObserver.Z1 microscope (Zeiss) equipped with filters for red fluorescent protein and cyan fluorescent protein fluorescence (63 HE and 47 HE; Zeiss). If fluorescence was present in half of the pollen grains, the offspring were counted as wild-type offspring; if fluorescence was not present, the offspring were counted as test offspring. The observed segregation ratio was tested against the expected 1:1 ratio using a χ^2 analysis.

In Vitro Pollen Tube Growth

Wild-type or mutant flowers were brushed together with WT* flowers onto solid pollen germination medium (0.01% [w/v] H_3BO_3, 5 mM $CaCl_2$, 1 mM $MgSO_4$, 5 mM KCl, 10% [w/v] Suc, and 1% [w/v] SeaPlaque GTG agarose, pH 7.75) on a microscope slide and incubated for 3 h in a dark, humid chamber at 22°C (Boavida and McCormick, 2007). Pollen tubes were observed on the AxioObserver.Z1 microscope (Zeiss) equipped with filters for YFP fluorescence (46 HE; Zeiss) and DIC optics. Images were captured using a CCD camera (Orca ER; Hamamatsu Photonics) operated by OpenLab5 software (Improvision/Perkin Elmer). For pollen tube length measurements, DIC images were captured using a 10× objective, and tube lengths were measured using OpenLab5 software. For pollen tube growth rate measurements, DIC time-lapse images were taken at 10-s intervals for 1.5 min using a 40× objective. Growth rate was calculated by measuring the amount of elongation that occurred within 1 min using OpenLab5 software. Wild-type and mutant measurements for tube length and growth rate were adjusted to the WT* measurements for each slide. Specifically, the average of all WT* measurements was divided by the average WT* measurements from each slide to obtain a correction factor for the test sample on each slide. The wild-type or mutant measurements for each slide were multiplied by the corresponding correction factor. This correction allowed for measurements from multiple replicates of the same genotype to be combined for the analysis. Mutants that were statistically different from the wild type were identified by an ordinary one-way ANOVA with Dunnett's correction for multiple comparisons using Prism 6 software (GraphPad).

In Vivo Pollen Tube Growth

Pollen tube growth in vivo was visualized by staining callose in pollen tube walls with Aniline Blue (Mori et al., 2006). Wild-type or mutant pollen was used to pollinate *ms1* flowers. Pollinated pistils were removed at various time points after pollination and placed in a fixing solution (3:1, ethanol:acetic acid). The pistils were aspirated and left in the fixing solution overnight. The fixed pistils were rehydrated by soaking for 10 min in each of the following solutions: 70% ethanol, 50% ethanol, 30% ethanol, and deionized water. The pistils were softened overnight in 8 M NaOH and washed for 10 min in deionized water. Aniline Blue solution (0.11% aniline blue in 0.1 M K_2HPO_4, pH approximately 11) was added, and the samples were covered with aluminum foil for 2 h. The Aniline Blue solution was made 3 d prior to use and was stored at 4°C. Immediately before use, glycerol was added to the Aniline Blue solution to a final concentration of 2%. After the 2-h incubation, the pistils were transferred to microscope slides. A small amount of Aniline Blue solution was added to each slide before placing a coverslip on it.

The pollen tubes in the pistils were observed using a 20× objective on an Axiovert 200M microscope (Zeiss) equipped with filters for 4′,6-diamino-phenylindole fluorescence (62002; Chroma). Images covering the length of each pistil were captured using a CCD camera (Orca ER; Hamamatsu Photonics) using OpenLab5 software (Improvision/Perkin Elmer). Using OpenLab5 software, the farthest distance traveled by a pollen tube was measured for each pistil. This was the distance from the highest (farthest from the style) pollen grain on the stigma to the lowest (farthest from the style) pollen tube tip in the ovary (Supplemental Fig. S2). Pollen tubes were not clearly visible in the style; therefore, if the pollen tube tips had not emerged from the style for a given pistil, the distance from the highest pollen grain on the stigma to halfway through the style was used for that measurement. Only pistils with more than five pollen grains on the stigma were used in the analysis, since low pollen density negatively affected pollen germination and growth (data not shown). Statistically significant differences were calculated by an ordinary one-way ANOVA with Dunnett's correction for multiple comparisons using Prism 6 software (GraphPad).

Organelle Movements

Pollen expressing either the peroxisome marker or the Golgi marker were germinated and grown in vitro, as described above. Pollen tubes were observed 3 to 7 h after setup using a 63× (1.4 numerical aperture [NA]) Plan-Apo oil-immersion objective on an Axiovert 200M microscope (Zeiss) equipped with filters for YFP fluorescence (69308; Chroma). Using OpenLab5 software (Improvision/Perkin Elmer), images were captured for 2 min with 0.5-s intervals using a CCD camera (Orca ER; Hamamatsu Photonics). At least nine independent videos were analyzed per treatment. Most time-lapse images included only one pollen tube; however, in a few cases, multiple pollen tubes were imaged together. Time-lapse images always included the pollen tube tip (i.e. organelle movements were analyzed within the first 150 μm from the tip).

Image sequences were exported to ImageJ, and background subtraction was performed using the rolling-ball radius that yielded the largest signal-to-noise ratio as calculated by a custom macro (available upon request). Individual organelle velocities were measured using the Particle Tracker plug-in (Sbalzarini and Koumoutsakos, 2005) for ImageJ. For particle detection, the radius and cutoff were always set to 2 and 1, respectively, while the percentile was adjusted between 0.2% and 0.9% depending on the image sequence. For particle linking, the link range was always set to 1, and the displacement was set to 20 pixels for peroxisomes and 15 pixels for Golgi stacks corresponding to a maximal velocity of 8 and 6 $\mu m\ s^{-1}$. The displacement values chosen were based on the maximum speeds measured for peroxisomes and Golgi stacks by manual tracking using OpenLab5 software (Supplemental Fig. S3). All measured velocities from one time-lapse sequence were combined to examine the range of cumulative distributions observed for each genotype. Velocities were then combined by genotype, and significant differences in the cumulative distribution of velocities between the wild type and *myo11c1-1 myo11c2-1* were calculated by a Kolmogorov-Smirnov test using Prism 6 software (GraphPad).

For the analysis of cytoplasmic streaming in additional genotypes, sequences of DIC images were captured in 0.5-s intervals over a period of 2 min for 10 to 12 pollen tubes per genotype. Regions of active streaming were manually selected for kymograph analysis in each pollen tube. Within each kymograph, 10 clearly visible tracks were selected, and the speed of the particle was calculated from its horizontal (space) and vertical (time) displacement. Particle speeds were compared with the wild type using ordinary ANOVA with Dunnett's correction for multiple comparisons in Prism 6 software (GraphPad).

RabA4d Vesicle Accumulation and Movements

Pollen expressing YFP-RabA4d was observed 4 to 8 h after setup using a 100× (1.3 NA) Plan-Neofluar oil-immersion objective on an Axiovert 200M microscope (Zeiss) with YFP filters (69308; Chroma). Images near the midplane of the pollen tubes were captured in 0.5-min intervals for 2 min. To analyze vesicle movement, image sequences were imported into ImageJ, and a straight or segmented line along the center of the pollen tube was selected. After creation of the kymographs with the Reslice command, individual particles were traced by superimposing a straight line selection on clearly visible tracks. Particle velocities were derived from the angle of this line with the horizontal using standard trigonometric methods.

Actin Filament Analysis

Pollen tubes expressing YFP-FABD2 as an actin marker were imaged at different focal planes to capture the entire volume of the cell using a 100× (1.3 NA) Plan-Neofluar oil-immersion objective on an Axiovert 200M microscope (Zeiss) with YFP filters (69308; Chroma). Z-stacks were combined into a single image by maximal intensity projection. Actin filaments were identified using a custom algorithm in ImageJ similar to the one published by Higaki et al. (2010). Briefly, after rolling-ball background subtraction, images were convolved with a filter to enhance linear features (Sun and Vallotton, 2009), thresholded, and skeletonized, and pixel intensities were adjusted to reflect the signal intensity in the original image (Supplemental Fig. S5B). Parallelness was calculated based on pixel pair frequencies as described (Ueda et al., 2010).

To calculate orderliness, first the central axis (midline) of the pollen tube was determined with a custom algorithm in ImageJ. In most cases, this was based on an automated detection of the pollen tube area, but for some cells, this detection was not reliable and the cell area had to be provided by manual selection (Supplemental Fig. S5C). In the next step, the angle of all linear elements (pixels) along an actin filament relative to the closest spot on the midline was calculated. The angle measurements for both filament and midline were smoothed over a five-pixel range to minimize errors due to pixelation. Individual angle values were weighted by the brightness at the given position in order to put more emphasis on actin bundles that contain more individual filaments. Mean angle and SD were calculated on a whole-cell basis. Orderliness is the reciprocal of this SD. A custom ImageJ macro that automates all image-processing steps and calculations is available upon request.

Sequence data from this article can be found in the GenBank/EMBL data libraries under accession numbers listed in Table III.

Supplemental Data

The following supplemental materials are available.

Supplemental Figure S1. Pollen tube growth in vitro varied greatly.

Supplemental Figure S2. An Arabidopsis pistil stained with aniline blue.

Supplemental Figure S3. Manual tracking of Golgi stacks and peroxisomes confirms slower movements in *myo11c1 myo11c2* pollen tubes.

Supplemental Figure S4. Cytoplasmic streaming is only affected in *myo11c1-1 myo11c2-1* pollen tubes.

Supplemental Figure S5. Detection and measurement of actin filaments.

Supplemental Table S1. Amino acid sequence identity between different pollen myosins.

Supplemental Movie S1. Golgi stack movements in wild-type and *myo11c1 myo11c2* pollen tubes.

Supplemental Movie S2. Peroxisome movements in wild-type and *myo11c1 myo11c2* pollen tubes.

Supplemental Movie S3. Cytoplasmic streaming in wild-type and mutant pollen tubes.

Supplemental Movie S4. YFP-RabA4d movements in wild-type and *myo11c1 myo11c2* pollen tubes.

ACKNOWLEDGMENTS

We thank Dr. Ravi Palanivelu (University of Arizona) for the gift of the male-sterile line; Dr. Greg Copenhaver (University of North Carolina) for the gift of the fluorescently tagged lines; Xue Cai, K. Denise Kendall, Kenneth Hoang, Tanner Beard, and Ryan Wilson (all at the University of Tennessee) for assistance at various stages of this project; and Dr. Albrecht G. von Arnim (University of Tennessee) for critical comments on the article. This work would not have been possible without the excellent collection of T-DNA insertion lines at the Arabidopsis Biological Resource Center.

Received July 23, 2015; accepted September 10, 2015; published September 10, 2015.

LITERATURE CITED

Akkerman M, Overdijk EJR, Schel JHN, Emons AMC, Ketelaar T (2011) Golgi body motility in the plant cell cortex correlates with actin cytoskeleton organization. Plant Cell Physiol **52:** 1844–1855

Alonso JM, Stepanova AN, Leisse TJ, Kim CJ, Chen H, Shinn P, Stevenson DK, Zimmerman J, Barajas P, Cheuk R, et al (2003) Genome-wide insertional mutagenesis of *Arabidopsis thaliana*. Science **301:** 653–657

Avisar D, Prokhnevsky AI, Dolja VV (2008) Class VIII myosins are required for plasmodesmatal localization of a closterovirus Hsp70 homolog. J Virol **82:** 2836–2843

Batoko H, Zheng HQ, Hawes C, Moore I (2000) A rab1 GTPase is required for transport between the endoplasmic reticulum and Golgi apparatus and for normal Golgi movement in plants. Plant Cell **12:** 2201–2218

Boavida LC, McCormick S (2007) Temperature as a determinant factor for increased and reproducible in vitro pollen germination in Arabidopsis thaliana. Plant J **52:** 570–582

Boavida LC, Shuai B, Yu HJ, Pagnussat GC, Sundaresan V, McCormick S (2009) A collection of *Ds* insertional mutants associated with defects in male gametophyte development and function in *Arabidopsis thaliana*. Genetics **181:** 1369–1385

Bou Daher F, Geitmann A (2011) Actin is involved in pollen tube tropism through redefining the spatial targeting of secretory vesicles. Traffic **12:** 1537–1551

Bove J, Vaillancourt B, Kroeger J, Hepler PK, Wiseman PW, Geitmann A (2008) Magnitude and direction of vesicle dynamics in growing pollen tubes using spatiotemporal image correlation spectroscopy and fluorescence recovery after photobleaching. Plant Physiol **147:** 1646–1658

Cai C, Henty-Ridilla JL, Szymanski DB, Staiger CJ (2014) Arabidopsis myosin XI: a motor rules the tracks. Plant Physiol **166:** 1359–1370

Chebli Y, Kroeger J, Geitmann A (2013) Transport logistics in pollen tubes. Mol Plant **6:** 1037–1052

Chenouard N, Smal I, de Chaumont F, Maška M, Sbalzarini IF, Gong Y, Cardinale J, Carthel C, Coraluppi S, Winter M, et al (2014) Objective comparison of particle tracking methods. Nat Methods **11:** 281–289

Crawford BC, Yanofsky MF (2011) *HALF FILLED* promotes reproductive tract development and fertilization efficiency in *Arabidopsis thaliana*. Development **138:** 2999–3009

Derksen J, Knuiman B, Hoedemaekers K, Guyon A, Bonhomme S, Pierson ES (2002) Growth and cellular organization of *Arabidopsis* pollen tubes *in vitro*. Sex Plant Reprod **15:** 133–139

Francis KE, Lam SY, Harrison BD, Bey AL, Berchowitz LE, Copenhaver GP (2007) Pollen tetrad-based visual assay for meiotic recombination in *Arabidopsis*. Proc Natl Acad Sci USA **104:** 3913–3918

Franke WW, Herth W, Vanderwoude WJ, Morré DJ (1972) Tubular and filamentous structures in pollen tubes: possible involvement as guide elements in protoplasmic streaming and vectorial migration of secretory vesicles. Planta **105:** 317–341

Furt F, Lemoi K, Tüzel E, Vidali L (2012) Quantitative analysis of organelle distribution and dynamics in *Physcomitrella patens* protonemal cells. BMC Plant Biol **12:** 70

Furt F, Liu YC, Bibeau JP, Tüzel E, Vidali L (2013) Apical myosin XI anticipates F-actin during polarized growth of *Physcomitrella patens* cells. Plant J **73:** 417–428

Golomb L, Abu-Abied M, Belausov E, Sadot E (2008) Different subcellular localizations and functions of Arabidopsis myosin VIII. BMC Plant Biol **8:** 3

Hajdukiewicz P, Svab Z, Maliga P (1994) The small, versatile pPZP family of *Agrobacterium* binary vectors for plant transformation. Plant Mol Biol **25:** 989–994

Haraguchi T, Tominaga M, Matsumoto R, Sato K, Nakano A, Yamamoto K, Ito K (2014) Molecular characterization and subcellular localization of *Arabidopsis* class VIII myosin, ATM1. J Biol Chem **289:** 12343–12355

Heslop-Harrison J, Heslop-Harrison Y (1989) Cytochalasin effects on structure and movement in the pollen tube of Iris. Sex Plant Reprod **2:** 27–37

Heslop-Harrison J, Heslop-Harrison Y (1990) Dynamic aspects of the apical zonation in the angiosperm pollen tube. Sex Plant Reprod **3:** 187–194

Higaki T, Kutsuna N, Sano T, Kondo N, Hasezawa S (2010) Quantification and cluster analysis of actin cytoskeletal structures in plant cells: role of actin bundling in stomatal movement during diurnal cycles in Arabidopsis guard cells. Plant J **61:** 156–165

Jiang SY, Cai M, Ramachandran S (2007) *ORYZA SATIVA MYOSIN XI B* controls pollen development by photoperiod-sensitive protein localizations. Dev Biol **304:** 579–592

Kinkema M, Schiefelbein J (1994) A myosin from a higher plant has structural similarities to class V myosins. J Mol Biol **239:** 591–597

Kohno T, Shimmen T (1988) Accelerated sliding of pollen tube organelles along Characeae actin bundles regulated by Ca^{2+}. J Cell Biol **106:** 1539–1543

Koornneef M, van Eden J, Hanhart CJ, Stam P, Braaksma FJ, Feenstra WJ (1983) Linkage map of *Arabidopsis thaliana*. J Hered **74:** 265–272

Lee YJ, Szumlanski A, Nielsen E, Yang Z (2008) Rho-GTPase-dependent filamentous actin dynamics coordinate vesicle targeting and exocytosis during tip growth. J Cell Biol **181:** 1155–1168

Li JF, Nebenführ A (2007) Organelle targeting of myosin XI is mediated by two globular tail subdomains with separate cargo binding sites. J Biol Chem **282:** 20593–20602

Li JF, Nebenführ A (2008) Inter-dependence of dimerization and organelle binding in myosin XI. Plant J **55:** 478–490

Madison SL, Nebenführ A (2013) Understanding myosin functions in plants: are we there yet? Curr Opin Plant Biol **16:** 710–717

Mascarenhas JP, Lafountain J (1972) Protoplasmic streaming, cytochalasin B, and growth of the pollen tube. Tissue Cell **4:** 11–14

Mori T, Kuroiwa H, Higashiyama T, Kuroiwa T (2006) GENERATIVE CELL SPECIFIC 1 is essential for angiosperm fertilization. Nat Cell Biol **8:** 64–71

Mühlhausen S, Kollmar M (2013) Whole genome duplication events in plant evolution reconstructed and predicted using myosin motor proteins. BMC Evol Biol **13:** 202

Nelson BK, Cai X, Nebenführ A (2007) A multicolored set of in vivo organelle markers for co-localization studies in Arabidopsis and other plants. Plant J **51:** 1126–1136

Odronitz F, Kollmar M (2007) Drawing the tree of eukaryotic life based on the analysis of 2,269 manually annotated myosins from 328 species. Genome Biol **8:** R196

Ojangu EL, Järve K, Paves H, Truve E (2007) *Arabidopsis thaliana* myosin XIK is involved in root hair as well as trichome morphogenesis on stems and leaves. Protoplasma **230:** 193–202

Ojangu EL, Tanner K, Pata P, Järve K, Holweg CL, Truve E, Paves H (2012) Myosins XI-K, XI-1, and XI-2 are required for development of pavement cells, trichomes, and stigmatic papillae in *Arabidopsis*. BMC Plant Biol **12:** 81

Park E, Nebenführ A (2013) Myosin XIK of *Arabidopsis thaliana* accumulates at the root hair tip and is required for fast root hair growth. PLoS One **8:** e76745

Parton RM, Fischer-Parton S, Watahiki MK, Trewavas AJ (2001) Dynamics of the apical vesicle accumulation and the rate of growth are related in individual pollen tubes. J Cell Sci **114:** 2685–2695

Peremyslov VV, Mockler TC, Filichkin SA, Fox SE, Jaiswal P, Makarova KS, Koonin EV, Dolja VV (2011) Expression, splicing, and evolution of the myosin gene family in plants. Plant Physiol **155:** 1191–1204

Peremyslov VV, Prokhnevsky AI, Avisar D, Dolja VV (2008) Two class XI myosins function in organelle trafficking and root hair development in Arabidopsis. Plant Physiol **146:** 1109–1116

Peremyslov VV, Prokhnevsky AI, Dolja VV (2010) Class XI myosins are required for development, cell expansion, and F-actin organization in *Arabidopsis*. Plant Cell **22:** 1883–1897

Prokhnevsky AI, Peremyslov VV, Dolja VV (2008) Overlapping functions of the four class XI myosins in Arabidopsis growth, root hair elongation, and organelle motility. Proc Natl Acad Sci USA **105:** 19744–19749

Reddy ANS, Day IS (2001) Analysis of the myosins encoded in the recently completed Arabidopsis thaliana genome sequence. Genome Biol **2:** research0024.1–research0024.17

Reichelt S, Knight AE, Hodge TP, Baluska F, Samaj J, Volkmann D, Kendrick-Jones J (1999) Characterization of the unconventional myosin VIII in plant cells and its localization at the post-cytokinetic cell wall. Plant J **19:** 555–567

Roy B, Copenhaver GP, von Arnim AG (2011) Fluorescence-tagged transgenic lines reveal genetic defects in pollen growth: application to the eIF3 complex. PLoS One **6:** e17640

Saint-Jore-Dupas C, Nebenführ A, Boulaflous A, Follet-Gueye ML, Plasson C, Hawes C, Driouich A, Faye L, Gomord V (2006) Plant *N*-glycan processing enzymes employ different targeting mechanisms for their spatial arrangement along the secretory pathway. Plant Cell **18:** 3182–3200

Sattarzadeh A, Franzen R, Schmelzer E (2008) The *Arabidopsis* class VIII myosin ATM2 is involved in endocytosis. Cell Motil Cytoskeleton **65:** 457–468

Sbalzarini IF, Koumoutsakos P (2005) Feature point tracking and trajectory analysis for video imaging in cell biology. J Struct Biol **151:** 182–195

Sebé-Pedrós A, Grau-Bové X, Richards TA, Ruiz-Trillo I (2014) Evolution and classification of myosins, a paneukaryotic whole-genome approach. Genome Biol Evol **6:** 290–305

Shimmen T (2007) The sliding theory of cytoplasmic streaming: fifty years of progress. J Plant Res **120:** 31–43

Sparkes I (2011) Recent advances in understanding plant myosin function: life in the fast lane. Mol Plant **4:** 805–812

Su H, Zhu J, Cai C, Pei W, Wang J, Dong H, Ren H (2012) FIMBRIN1 is involved in lily pollen tube growth by stabilizing the actin fringe. Plant Cell **24:** 4539–4554

Sun C, Vallotton P (2009) Fast linear feature detection using multiple directional non-maximum suppression. J Microsc **234:** 147–157

Szumlanski AL, Nielsen E (2009) The Rab GTPase RabA4d regulates pollen tube tip growth in *Arabidopsis thaliana*. Plant Cell **21:** 526–544

Tominaga M, Kojima H, Yokota E, Nakamori R, Anson M, Shimmen T, Oiwa K (2012) Calcium-induced mechanical change in the neck domain alters the activity of plant myosin XI. J Biol Chem **287:** 30711–30718

Tominaga M, Kojima H, Yokota E, Orii H, Nakamori R, Katayama E, Anson M, Shimmen T, Oiwa K (2003) Higher plant myosin XI moves processively on actin with 35 nm steps at high velocity. EMBO J **22:** 1263–1272

Ueda H, Yokota E, Kutsuna N, Shimada T, Tamura K, Shimmen T, Hasezawa S, Dolja VV, Hara-Nishimura I (2010) Myosin-dependent endoplasmic reticulum motility and F-actin organization in plant cells. Proc Natl Acad Sci USA **107:** 6894–6899

Van Damme D, Bouget FY, Van Poucke K, Inzé D, Geelen D (2004) Molecular dissection of plant cytokinesis and phragmoplast structure: a survey of GFP-tagged proteins. Plant J **40:** 386–398

Vidali L, Burkart GM, Augustine RC, Kerdavid E, Tüzel E, Bezanilla M (2010) Myosin XI is essential for tip growth in *Physcomitrella patens*. Plant Cell **22:** 1868–1882

Vidali L, McKenna ST, Hepler PK (2001) Actin polymerization is essential for pollen tube growth. Mol Biol Cell **12:** 2534–2545

Vivian-Smith A, Luo M, Chaudhury A, Koltunow A (2001) Fruit development is actively restricted in the absence of fertilization in *Arabidopsis*. Development **128:** 2321–2331

Voigt B, Timmers ACJ, Samaj J, Müller J, Baluska F, Menzel D (2005) GFP-FABD2 fusion construct allows in vivo visualization of the dynamic actin cytoskeleton in all cells of *Arabidopsis* seedlings. Eur J Cell Biol **84:** 595–608

Weigel D, Glazebrook J, editors (2002) Arabidopsis: A Laboratory Manual. Cold Spring Harbor Laboratory Press, Cold Spring Harbor, NY

Wilson ZA, Morroll SM, Dawson J, Swarup R, Tighe PJ (2001) The *Arabidopsis MALE STERILITY1* (*MS1*) gene is a transcriptional regulator of male gametogenesis, with homology to the PHD-finger family of transcription factors. Plant J **28:** 27–39

Wu SZ, Bezanilla M (2014) Myosin VIII associates with microtubules ends and together with actin plays a role in guiding plant cell division. eLife **3:** e03498

Wu Y, Yan J, Zhang R, Qu X, Ren S, Chen N, Huang S (2010) *Arabidopsis* FIMBRIN5, an actin bundling factor, is required for pollen germination and pollen tube growth. Plant Cell **22:** 3745–3763

Yokota E, McDonald AR, Liu B, Shimmen T, Palevitz BA (1995) Localization of a 170 kDa myosin heavy chain in plant cells. Protoplasma **185:** 178–187

Yokota E, Muto S, Shimmen T (1999) Inhibitory regulation of higher-plant myosin by Ca^{2+} ions. Plant Physiol **119:** 231–240

Yokota E, Shimmen T (1994) Isolation and characterization of plant myosin from pollen tubes of lily. Protoplasma **177:** 152–162

Yuan Z, Chen H, Chen Q, Omura T, Xie L, Wu Z, Wei T (2011) The early secretory pathway and an actin-myosin VIII motility system are required for plasmodesmatal localization of the NSvc4 protein of Rice stripe virus. Virus Res **159:** 62–68

Zhu L, Zhang Y, Kang E, Xu Q, Wang M, Rui Y, Liu B, Yuan M, Fu Y (2013) MAP18 regulates the direction of pollen tube growth in *Arabidopsis* by modulating F-actin organization. Plant Cell **25:** 851–867